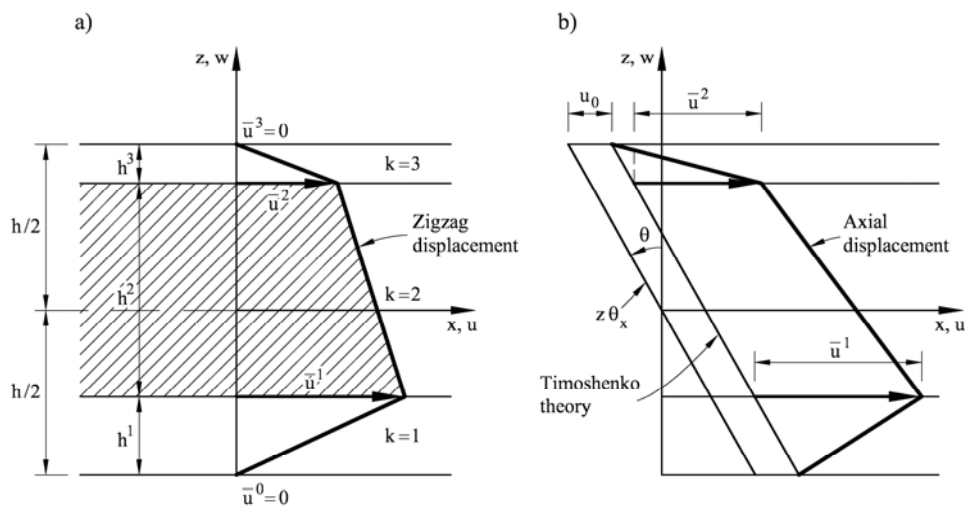# Two-Noded Beam Element for Composite and Sandwich Beams using Timoshenko Theory and Refined Zigzag Kinematics

E. Oñate
A. Eijo
S. Oller

# Two-Noded Beam Element for Composite and Sandwich Beams using Timoshenko Theory and Refined Zigzag Kinematics

E. Oñate
A. Eijo
S. Oller

# TWO-NODED BEAM ELEMENT FOR COMPOSITE AND SANDWICH BEAMS USING TIMOSHENKO THEORY AND REFINED ZIGZAG KINEMATICS

**E. Oñate, A. Eijo and S. Oller**

International Center for Numerical Methods in Engineering (CIMNE)

School of Civil Engineering

Technical University of Catalonia (UPC)

Campus Norte UPC, 08034 Barcelona, Spain

onate@cimne.upc.edu, www.cimne.com/eo

**Abstract.** The so-called zigzag theory has been developed in recent years as an extension of the classical layer-wise theory for modeling composite laminated beams, plates and shells. An advantage of the zigzag theory is that the number of kinematic variables is independent of the number of layers. In this work we present a simple linear two-noded beam element adequate for the analysis of composite and sandwich beams based on the combination of classical Timoshenko beam theory and the refined zigzag kinematics recently proposed by Tessler *et al.* [19]. The accuracy of the new beam element is tested in a number of examples of applications for composite laminated beams.

## 1 INTRODUCTION

Timoshenko beam theory (TBT) [1] produces inadequate predictions when applied to relatively thick composite laminated beams with material layers that have highly dissimilar stiffness characteristics. Even with a judiciously chosen shear correction factor, Timoshenko theory tends to underestimate the axial stress at the top and bottom outer fibers of a beam. Also, along the layer interfaces of a laminated beam the transverse shear stresses predicted often exhibit erroneous discontinuities. These difficulties are due to the higher complexity of the "true" variation of the in-plane displacement field across a highly heterogeneous beam cross-section.

Indeed to achieve accurate computational results, 3D finite element analyses are often preferred over beam, plate and shell models that are based on first order shear deformation theories, such as the Timoshenko and Euler-Bernouilli theories. For composite laminates with hundred of layers, however, 3D modelling becomes prohibitely expensive, especially for non linear and progressive failure analyses.

The need for composite laminated beam, plate and shell theories with better predictive capabilities has led to the development of the so-called *higher order* theories. A review can be found in [2]. In refined beam theories higher-order kinematic terms with respect to the beam depth are added to the expression for the in-plane

displacement and, in some case, to the expressions for the deflection.

The prediction of the correct shear and axial stresses for thick and highly heterogenous composite laminated and sandwich structures can be improved by using the so-called *layer-wise* theory. In this theory the thickness coordinate is split into a number of *analysis layers* that may or not coincide with the number of laminate plies. The kinematics are independently described within each layer and certain physical continuity requirements are enforced [2, 3, 4].

A drawback of layer-wise theory is that the number of kinematic variables depends on the number of analysis layers. The layer displacements can be condensed at each section in terms of the axial displacement for the top layer during the equation solution process [5, 6]. The displacement condensation processes can be however expensive for problems involving many analysis layers.

The so called zigzag theory has been developed in recent years as an effort for enhancing the classical layer-wise theory for modeling composite laminated beams, plates and shells. An advantage of the zigzag theory is that the number of kinematic variables is independent of the number of layers. In this work we present a simple linear two-noded beam element adequate for the analysis of composite and sandwich beams based on the combination of classical Timoshenko beam theory and the refined zigzag kinematics proposed by Tessler *et al.* [19]. The accuracy of the new beam element is tested in a number of examples of application for composite laminated beams.

## 2  GENERAL CONCEPTS OF ZIGZAG BEAM THEORY

The so-called zigzag beam theories are a sub-class of the general layer-wise theory. They assume a zigzag pattern for the axial displacements and enforce continuity of the transverse shear stresses across the entire laminate depth. Importantly, *the number of kinematic variables in zigzag theories is independent of the number of layers*.

The kinematic field in zigzag beam theories can be generally written as

$$
\begin{aligned}
u^k(x,z) &= u_0(x) - z\theta(x) + \bar{u}^k(x,z) \\
w(x,z) &= w_0(x)
\end{aligned}
\tag{1a}
$$

where

$$
\bar{u}^k = \phi^k(z)\Psi(x) \quad , \quad k = 1, N
\tag{1b}
$$

is the zigzag displacement function.

In Eqs.(1) $N$ is the number of layers, superscript $k$ indicates quantities within the $k$th layer with $z_k \leq z \leq z_{k+1}$ and $z_k$ is the vertical coordinate of the $k$th interface. In Eq.(1a) the uniform axial displacement $u_0(x)$, the rotation $\theta(x)$ and the transverse deflection $w_0(x)$ are the primary kinematic variables of the underlying equivalent single-layer Timoshenko beam theory. In Eq.(1b) function $\phi^k(z)$ denotes *a piecewise linear zigzag function*, yet to be established, and $\Psi(x)$ is a primary kinematic variable that defines the *amplitude of the zigzag function* along the beam. Collectively, the interfacial axial displacement field has a zigzag distribution, as shown in Figure 1.
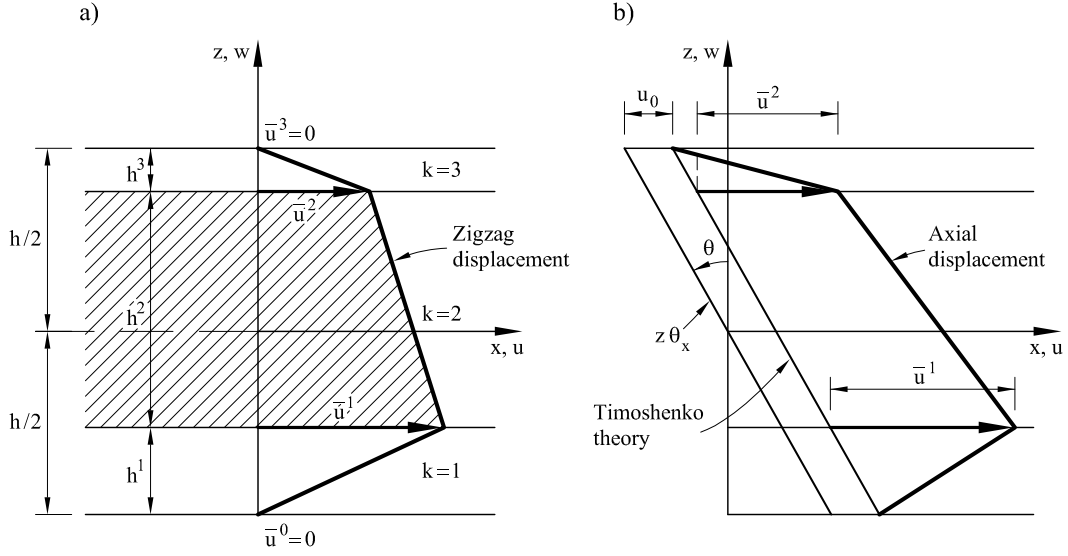
**Figure 1**: Distribution of the zigzag displacement and axial displacement in zigzag beam theory

The strain-displacement relations are derived by substituting Eq.(3a) into the expressions of classical Timoshenko beam theory, i.e.

$$\varepsilon_x^k = \frac{\partial u^k}{\partial x} = \frac{\partial u_0}{\partial x} - z\frac{\partial \theta}{\partial x} + \phi^k\frac{\partial \Psi}{\partial x} = [1, -z, \phi^k]\left\{\begin{array}{c} \dfrac{\partial u_0}{\partial x} \\[2mm] \dfrac{\partial \theta}{\partial x} \\[2mm] \dfrac{\partial \Psi}{\partial x} \end{array}\right\} = \mathbf{S}_p\hat{\boldsymbol{\varepsilon}}_p \qquad (2a)$$

$$\gamma_{xz}^k = \frac{\partial u^k}{\partial z} + \frac{\partial w}{\partial x} = \frac{\partial w_0}{\partial x} - \theta + \frac{\partial \phi^k}{\partial z}\Psi = \gamma + \beta^k\Psi = [1, \beta^k]\left\{\begin{array}{c} \gamma \\ \Psi \end{array}\right\} = \mathbf{S}_t\hat{\boldsymbol{\varepsilon}}_t \qquad (2b)$$

In Eq.s (2a) and (2b)

$$\begin{aligned} \mathbf{S}_p &= [1, -z, \phi^k] \quad , \quad \hat{\boldsymbol{\varepsilon}}_p = \left[\frac{\partial u_0}{\partial x}, \frac{\partial \theta}{\partial x}, \frac{\partial \Psi}{\partial x}\right]^T \\ \mathbf{S}_t &= [1, \beta^k] \quad , \qquad \hat{\boldsymbol{\varepsilon}}_t = [\gamma, \Psi]^T \end{aligned} \qquad (2c)$$

where $\hat{\boldsymbol{\varepsilon}}_p$ and $\hat{\boldsymbol{\varepsilon}}_t$ are the generalized in-plane and transverse shear strain vectors, respectively. Vector $\hat{\boldsymbol{\varepsilon}}_p$ contains the axial elongation $\left(\frac{\partial u_0}{\partial x}\right)$, the pseudo-curvature $\left(\frac{\partial \theta}{\partial x}\right)$ and the derivatives of the amplitude of the zigzag function $\left(\frac{\partial \Psi}{\partial x}\right)$. In $\hat{\boldsymbol{\varepsilon}}_t$, $\gamma = \frac{\partial w_0}{\partial x} - \theta$ is the average transverse shear strain of Timoshenko beam theory and $\beta^k = \frac{\partial \phi^k}{\partial z}$. Note that since $\phi^k(z)$ is piecewise linear, $\beta^k$ is constant across each layer.

For major principal material axes that are coincident with the beam $x$ axis, Hooke stress-strain relations for the $k$th orthotropic layer have the standard form

$$\sigma_x^k = E^k\varepsilon_x^k = E^k\mathbf{S}_p\hat{\boldsymbol{\varepsilon}}_p \qquad (3a)$$

$$\tau_{xz}^k = G^k\gamma_{xz}^k = G^k\mathbf{S}_t\hat{\boldsymbol{\varepsilon}}_t \qquad (3b)$$

3

where $E^k$ and $G^k$ are the axial and shear moduli for the $k$th layer, respectively.

Note that in the above equations we have distinguished all variables within a layer with superscript $k$.

Existing zigzag theories differ in the way they define the zigzag function $\phi^k(z)$ [7]–[10]. In the early zigzag theories for plates, Di Sciuva [7] enforced a constant shear stress across the entirely laminated thickness. This model was subsequently enhanced by adding a cubic in-plane displacement to the zigzag function [11, 12]. Di Sciuva theories require $C^1$ continuity for the deflection field, which is a drawback versus simpler $C^\circ$ continuous FEM approximations. Also Di Sciuva's theory runs into theoretical difficulties to satisfy equilibrium of forces at a clamped support.

Averill [13, 14] developed linear and cubic zigzag beam theory for Timoshenko beams and thus overcame the need for $C^1$ continuity. The continuity of the transverse shear stress across the laminate depth is enforced via a penalty method. However, Averill theory is also unable to model correctly clamped boundary conditions. For this reason, analytical and numerical (FEM) studies based on Averill theory have mainly focused on simple supported beams [13, 14].

A 2-noded beam element based on Euler-Bernouilli beam theory and an extension of Averill's zigzag theory including a cubic in-plane displacement field within each layer has been recently proposed by Alam and Upadhyay [15]. Good results are reported for cantilever and clamped composite and sandwich beams.

An assessment of different zigzag theories is reported in [16, 17, 18].

In this paper we present an efficient 2-noded beam element that combines Timoshenko beam theory and the refined zigzag theory recently presented by Tessler *et al.* [19]. This zigzag theory requires a simple $C^\circ$ continuous approximation for all the kinematic variables and overcomes most of the problems of Di Sciuva and Averill theories.

## 3 REFINED ZIGZAG THEORY

### 3.1 Zigzag kinematic

The key attributes of the refined zigzag theory proposed by Tessler *et al.* [] are, first, *the zigzag function vanishes at the top and bottom surfaces of the beam section* and does not requires full shear-stress continuity across the laminated-beam depth. Second, all boundary conditions can be modelled adequately. And third, $C^\circ$ continuity is only required for the FEM approximation of the kinematic variables.

Within each layer the zigzag function is expressed as

$$\phi^k = \frac{1}{2}(1-\xi)u^{k-1} + \frac{1}{2}(1+\xi)u^k = \frac{u^k + u^{k-1}}{2} + \frac{u^k - u^{k-1}}{2}\xi^k \qquad (4)$$

where $u^k$ and $u^{k-1}$ are the displacements of the $k$ and $k-1$ interface, respectively with $u^0 = u^N = 0$ and $\xi^k = \frac{2(z-z^{k-1})}{h^k} - 1$.

Collectively, the zigzag displacement function has the zigzag distribution shown in Figure 1a. Note that $\bar{u}^k$ vanishes at the top and bottom layers. The axial displacement field is plotted in Figure 1b.

The above form of $\phi^k$ gives

$$\beta^k = \frac{\partial \phi^k}{\partial z} = \frac{u^k - u^{k-1}}{h^k} \tag{5a}$$

and

$$\iint_A \beta^k dA = 0 \tag{5b}$$

Integrating Eq.(2b) over the cross section and using Eq.(5b) and the fact that $\Psi$ is independent of $z$ yields

$$\gamma = \frac{1}{A} \iint_A \gamma_{xz}^k dA \tag{6}$$

i.e. $\gamma$ represents the average shear strain of the cross section, as expected.

The shear strain-shear stress relationship of Eq.(3b) is written as

$$\tau_{xz}^k = G^k \eta + G^k (1 + \beta^k) \Psi \tag{7}$$

where $\eta = \gamma - \Psi$ is a difference function.

Clearly the distribution of $\tau_{xz}^k$ within each layer is constant, as $\eta$ is independent of the zigzag function and $\beta^k$ is constant (see Eq.(5a)).

The distribution of $\tau_{xz}^k$ is now enforced to be independent of the zigzag function. This can be achieved by constraining the term multiplying $\Psi$ in Eq.(7) to be constant, i.e.

$$G^k(1 + \beta^k) = G^{k+1}(1 + \beta^{k+1}) = G, \quad \text{constant} \tag{8}$$

This is equivalent to enforcing the interfacial continuity of the second term in the r.h.s. of Eq.(7).

From Eq.(8) we deduce

$$\beta^k = \frac{G}{G^k} - 1 \tag{9}$$

Substituting $\beta^k$ in the integral of Eq.(5b) gives

$$G = \left[ \frac{1}{A} \iint_A \frac{dA}{G^k} \right]^{-1} = \left[ h \sum_{k=1}^{N} \frac{h^k}{G^k} \right]^{-1} \tag{10}$$

where $h$ is the section depth. Substituting Eq.(9) into Eq.(5a) gives the following recursion relation for the layer interface displacements

$$\bar{u}_k = \sum_{i=1}^{k} h^i \beta^i \quad \text{with} \quad u^0 = u^N = 0 \tag{11}$$

Introducing Eq.(11) into (4) gives the expression for the zigzag function as

$$\phi^k = \frac{h^k \beta^k}{2}(\xi^k - 1) + \sum_{i=1}^{k} h^i \beta^i \tag{12}$$

Recall that superindex $k$ denotes the number of each material layer.

Function $\Psi$ can be interpreted as a weighted-average shear strain angle [19]. The value of $\Psi$ should be prescribed to zero at a clamped edge and left unprescribed at a free edge.

We recall that this theory does not enforce the continuity of the transverse shear stresses across the section. This is consistent with the kinematic freedom inherent in the lower order kinematic approximation of the underlying beam theory.

For homogeneous material $G^k = G$ and $\beta^k = 0$. Hence, the zigzag function $\phi^k$ vanishes and we recover the kinematic and constitutive expression of the standard Timoshenko composite laminated beam theory studied.

## 3.2 Constitutive relationship

The in-plane bending and transverse shear resultant stresses are defined as

$$\hat{\boldsymbol{\sigma}}_p = \left\{ \begin{array}{c} N \\ M \\ M_\phi \end{array} \right\} = \iint_A \mathbf{S}_p^T \sigma_x^k dA = \left( \iint_A \mathbf{S}_p^T \mathbf{S}_p E^k dA \right) \hat{\boldsymbol{\varepsilon}}_p = \hat{\mathbf{D}}_p \hat{\boldsymbol{\varepsilon}}_p \qquad (13)$$

$$\hat{\boldsymbol{\sigma}}_t = \left\{ \begin{array}{c} Q \\ Q_\phi \end{array} \right\} = \iint_A \mathbf{S}_t^T \tau_{xz}^k dA = \left( \iint_A \mathbf{S}_t^T \mathbf{S}_t G_{xz}^k dA \right) \hat{\boldsymbol{\varepsilon}}_t = \hat{\mathbf{D}}_t \hat{\boldsymbol{\varepsilon}}_t \qquad (14)$$

In vectors $\hat{\boldsymbol{\sigma}}_p$ and $\hat{\boldsymbol{\sigma}}_t$, $N, M$ and $Q$ are respectively the axial force, the bending moment and the transverse shear force of standard beam theory, whereas $M_\phi$ and $Q_\phi$ are an additional bending moment and an additional shear force which are conjugate to the new generalized strains $\frac{\partial \Psi}{\partial x}$ and $\Psi$, respectively.

The generalized constitutive matrices $\hat{\mathbf{D}}_b$ and $\hat{\mathbf{D}}_t$ are

$$\hat{\mathbf{D}}_p = \iint_A E^k \begin{bmatrix} 1 & -z & \phi \\ -z & z^2 & -z\phi \\ \phi & -z\phi & \phi^2 \end{bmatrix} dA \quad , \quad \hat{\mathbf{D}}_t = \begin{bmatrix} D_s & -\lambda \\ -\lambda & \lambda \end{bmatrix} \qquad (15a)$$

with

$$D_s = \iint_A G^k dA \quad , \quad \lambda = D_s - GA \qquad (15b)$$

In the derivation of the expression for $\hat{\mathbf{D}}_s$ we have used the definition of $\beta^k$ of Eq.(9).

The generalized constitutive equation can be written as

$$\hat{\boldsymbol{\sigma}} = \left\{ \begin{array}{c} \hat{\boldsymbol{\sigma}}_p \\ \hat{\boldsymbol{\sigma}}_t \end{array} \right\} = \hat{\mathbf{D}}\hat{\boldsymbol{\varepsilon}} = \hat{\mathbf{D}} \left\{ \begin{array}{c} \hat{\boldsymbol{\varepsilon}}_p \\ \hat{\boldsymbol{\varepsilon}}_t \end{array} \right\} \qquad \text{with} \quad \hat{\mathbf{D}} = \begin{bmatrix} \hat{\mathbf{D}}_p & \mathbf{0} \\ \mathbf{0} & \hat{\mathbf{D}}_t \end{bmatrix} \qquad (16)$$

## 3.3 Virtual work expression

The virtual work expression for a distributed load $q$ is

$$\iiint_V (\delta\varepsilon_x^k \sigma_x^k + \delta\gamma_{xz}^k \tau_x^k) dV - \int_l \delta w q dA = 0 \qquad (17)$$

The l.h.s. of Eq.(17) contains the internal virtual work performed by the axial and tangential stresses and the r.h.s. is the external virtual work carried out by the distributed load. $V$ and $l$ are the volume and length of the beam, respectively.

Substituting Eqs.(3) into the expression for the virtual internal work and using Eqs.(13) and (14) gives

$$\iiint_V \left( \delta\varepsilon_x^k \sigma_x^k + \delta\gamma_{xz}^k \tau_x^k \right) dV = \iiint_V \left( \delta\hat{\boldsymbol{\varepsilon}}_p^T \mathbf{S}_p^T \sigma_x^k + \delta\hat{\boldsymbol{\varepsilon}}_t^T \mathbf{S}_t^T \tau_{xz}^k \right) dV =$$

$$= \int_l \left( \delta\hat{\boldsymbol{\varepsilon}}_p^T \hat{\boldsymbol{\sigma}}_p + \delta\hat{\boldsymbol{\varepsilon}}_t^T \hat{\boldsymbol{\sigma}}_t \right) dx \tag{18}$$

The virtual work is therefore written as

$$\int_l \left( \delta\hat{\boldsymbol{\varepsilon}}_p^T \hat{\boldsymbol{\sigma}}_p + \delta\hat{\boldsymbol{\varepsilon}}_t^T \hat{\boldsymbol{\sigma}}_t \right) dx - \int_l \delta w q \, dx = 0 \tag{19}$$

## 4   TWO-NODED LTZZ BEAM ELEMENT

The kinematic variables are $u_0, w_0, \theta$ and $\Psi$. They can be discretized using 2-noded linear $C^\circ$ beam elements of length $l^e$ in the standard form as

$$\mathbf{u} = \left\{ \begin{array}{c} u_0 \\ w_0 \\ \theta \\ \Psi \end{array} \right\} = \sum_{i=1}^{2} N_i \mathbf{a}_i = \mathbf{N} \mathbf{a}^e \tag{20}$$

with

$$\mathbf{N} = [N_1 \mathbf{I}_4, N_2 \mathbf{I}_4] \quad, \quad \mathbf{a}^e = \left\{ \begin{array}{c} \mathbf{a}_1 \\ \mathbf{a}_2 \end{array} \right\} \quad, \quad \mathbf{a}_i = \left\{ \begin{array}{c} u_{0_i} \\ w_{0_i} \\ \theta_i \\ \Psi_i \end{array} \right\} \tag{21}$$

where $N_i = \frac{1}{2}(1 + \eta\eta_i)$ with $\eta = 1 - \frac{2x}{l^e}$ are the standard one-dimensional linear shape functions, $\mathbf{a}_i$ is the vector of nodal kinematic variables and $\mathbf{I}_4$ is the $4 \times 4$ unit matrix.

Substituting Eq.(22) into the generalized strain vectors in Eq.(4c) gives

$$\hat{\boldsymbol{\varepsilon}}_p = \mathbf{B}_p \mathbf{a}^e \quad, \quad \hat{\boldsymbol{\varepsilon}}_t = \mathbf{B}_t \mathbf{a}^e \tag{22}$$

The generalized strain matrices $\mathbf{B}_p$ and $\mathbf{B}_t$ are

$$\mathbf{B}_p = [\mathbf{B}_{p_1}, \mathbf{B}_{p_2}] \quad, \quad \mathbf{B}_t = [\mathbf{B}_{t_1}, \mathbf{B}_{t_2}] \tag{23a}$$

with

$$\mathbf{B}_{p_i} = \begin{bmatrix} \dfrac{\partial N_i}{\partial x} & 0 & 0 & 0 \\ 0 & 0 & \dfrac{\partial N_i}{\partial x} & 0 \\ 0 & 0 & 0 & \dfrac{\partial N_i}{\partial x} \end{bmatrix} \tag{23b}$$

$$\mathbf{B}_{t_i} = \begin{bmatrix} 0 & \dfrac{\partial N_i}{\partial x} & -N_i & 0 \\ -- & -- & -- & -- \\ 0 & 0 & 0 & N_i \end{bmatrix} = \begin{bmatrix} \mathbf{B}_{s_i} \\ -- \\ \mathbf{B}_{\psi_i} \end{bmatrix} \tag{23c}$$

where $\mathbf{B}_{p_i}$ and $\mathbf{B}_{t_i}$ are the in-plane and transverse shear strain matrices for node $i$.

The virtual displacement and generalized strain fields are expressed in terms of the virtual nodal kinematic variables as

$$\delta\mathbf{u} = \mathbf{N}\delta\mathbf{a}^e \quad , \quad \delta\hat{\boldsymbol{\varepsilon}}_p = \mathbf{B}_p\delta\mathbf{a}^e \quad , \quad \delta\hat{\boldsymbol{\varepsilon}}_t = \mathbf{B}_t\delta\mathbf{a}^e \tag{24}$$

The discretized equilibrium equations are obtained by substituting Eqs.(13), (14), (20), (22) and (24) into the virtual work expression (19). After simplification of the virtual nodal kinematic variables, the following standard matrix equation is obtained

$$\mathbf{Ka} - \mathbf{f} = 0 \tag{25}$$

where $\mathbf{a}$ is the vector of nodal kinematic variables for the whole mesh.

The stiffness matrix $\mathbf{K}$ and the equivalent nodal force vector $\mathbf{f}$ are obtained by assembling the element contributions $\mathbf{K}^e$ and $\mathbf{f}^e$ given by

$$\mathbf{K}^e = \mathbf{K}^e_p + \mathbf{K}^e_t \tag{26}$$

with

$$\mathbf{K}^e_{p_{ij}} = \int_{l^e} \mathbf{B}^T_{p_i}\hat{\mathbf{D}}_p\mathbf{B}_{p_j}dx \quad , \quad \mathbf{K}^e_{t_{ij}} = \int_{l^e} \mathbf{B}^T_{t_i}\hat{\mathbf{D}}_t\mathbf{B}_{t_j}dx \tag{27}$$

and

$$\mathbf{f}^e = \int_{l^e} N_i q[1,0,0,0]^T dx \tag{28}$$

Matrix $\mathbf{K}^e_p$ is integrated with a one-point numerical quadrature which is exact in this case. Full integration of matrix $\mathbf{K}^e_t$ requires a two-point Gauss quadrature. This however leads to shear locking for slender composite laminated beams (see Section 5).

In order to asses the influence of the reduced integration of matrix $\mathbf{K}^e_t$ for solving the transverse shear locking problem we split $\mathbf{K}^e_t$ as follows

$$\mathbf{K}^e_t = \mathbf{K}^e_s + \mathbf{K}^e_\psi + \mathbf{K}^e_{s\psi} + [\mathbf{K}^e_{s\psi}]^T \tag{29a}$$

with

$$\mathbf{K}^e_{s_{ij}} = \int_{l^e} D_s\mathbf{B}^T_{s_i}\mathbf{B}_{s_j}dx \quad , \quad \mathbf{K}^e_{\psi_{ij}} = \int_{l^e} \lambda\mathbf{B}^T_{\psi_i}\mathbf{B}_{\psi_j}dx \tag{29b}$$

$$\mathbf{K}^e_{s\psi_{ij}} = \int_{l^e} (-\lambda)\mathbf{B}^T_{s_i}\mathbf{B}_{\psi_j}dx$$

where $\mathbf{B}_{s_i}$ and $\mathbf{B}_{\psi_i}$ are defined in Eq.(23c) and $D_s$ and $\lambda$ are given in Eq.(15b).

The new beam element is termed LTZZ (for **L**inear **T**imoshenko **Z**ig**Z**ag element).

A study of the accuracy of the LTZZ beam element for analysis of slender laminated beams using one and two-point quadratures for integrating matrices $\mathbf{K}^e_s$, $\mathbf{K}^e_\psi$ and $\mathbf{K}^e_{s\psi}$ is presented in the next section.
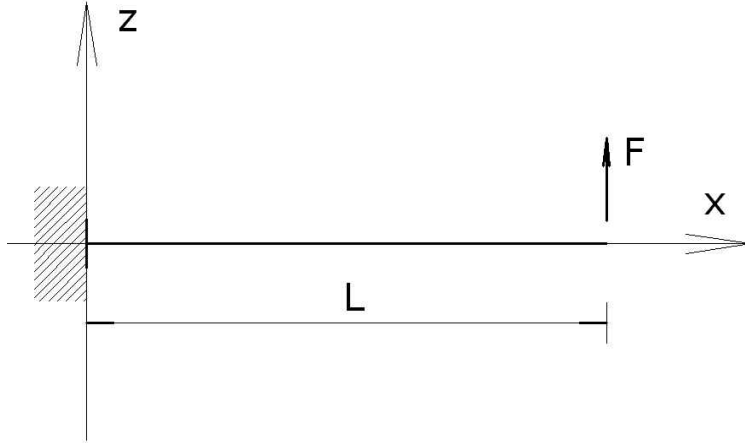
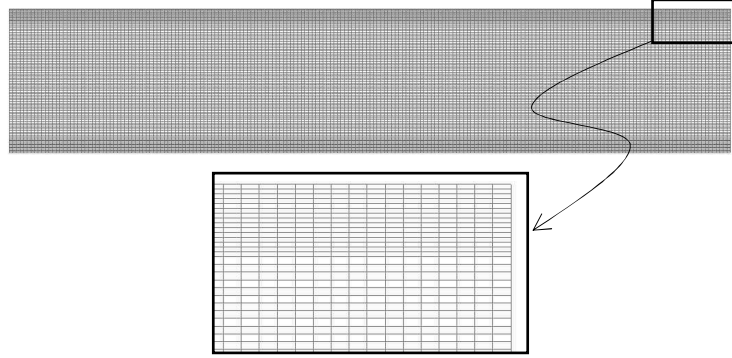**Figure 2**: Cantilever beam under point load



**Figure 3**: Mesh of 27000 4-noded plane stress rectangular elements for analysis of cantilever and simple supported beams

## 5   STUDY OF SHEAR LOCKING FOR THE LTZZ BEAM ELEMENT

We study the performance of the LTZZ beam element for the analysis of a cantilever beam of length $L$ under an end point load (Figure 2). The beam is formed by a symmetric three-layered material whose properties are listed on Table 1. The analysis is performed for four slenderness ratios: $\lambda = 5, 10, 50, 100$ ($\lambda = L/h$) using a mesh of 100 LTZZ beam elements. Results for the LTZZ element are labelled "ZZ" in the figures.

The same beam was analized using a mesh of 27000 four-noded plane stress rectangles for comparison purposes (Figure 3). Results for the plane stress analysis are labeled "PS" in the figures.

Figure 4 shows the ratio $k$ between the end node deflection obtained with the LTZZ element ($w_{zz}$) and with the plane stress quadrilateral ($w_{ps}$) (i.e. $k = \frac{w_{zz}}{w_{ps}}$). Results for the LTZZ element have been obtained using *exact* two-point integration for all terms of matrix $\mathbf{K}_t^e$ (Eq.(27)) and a one-point *reduced* integration for the following three groups of matrices: $\mathbf{K}_s^e$; $\mathbf{K}_s^e$ and $\mathbf{K}_{s\psi}^e$; and $\mathbf{K}_s$, $\mathbf{K}_{s\psi}^e$ and $\mathbf{K}_{\psi}^e$ (Eqs.(29b)).

Labels "*all*", "*S*", "*SPsi*" and "*Psi*" in Figures 4–7 refer to matrices $\mathbf{K}_t^e$, $\mathbf{K}_s^e$,

|  | Composite material properties | | |
|---|---|---|---|
|  | Layer 1 (bottom) | Layer 2 (core) | Layer 3 (top) |
| h [mm] | 6.6667 | 6.6667 | 6.6667 |
| E [MPa] | 2.19E5 | 2.19E3 | 2.19E5 |
| G [MPa] | 0.876E5 | 8.80E2 | 0.876E5 |

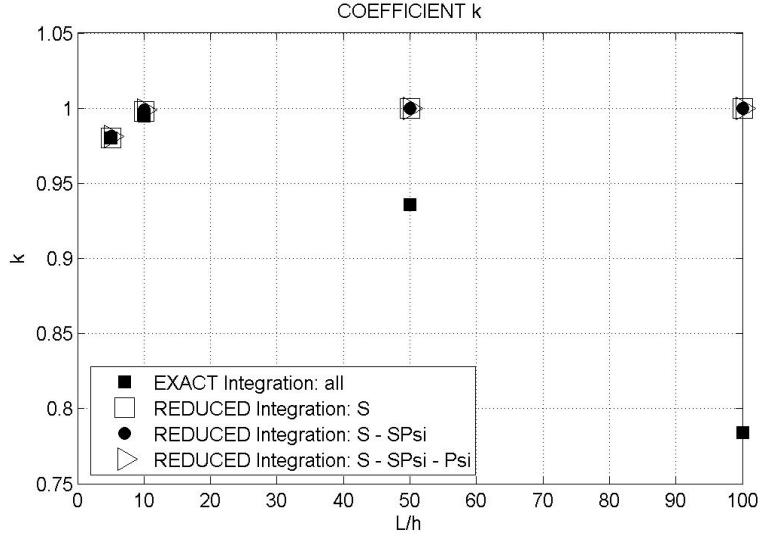**Table 1**: Symmetric 3-layered cantilever beam. Material properties for shear locking study



**Figure 4**: $k$ ratio $\left(k = \frac{w_{zz}}{w_{ps}}\right)$ versus $L/h$ for cantilever beam under point load analyzed with the LTZZ element. Labels "*all*", $S$, $SPsi$ and $Psi$ refer to matrices $\mathbf{K}_t^e$, $\mathbf{K}_s^e$, $\mathbf{K}_{s\psi}^e$ and $\mathbf{K}_\psi^e$, respectively

$\mathbf{K}_{s\psi}^e$ and $\mathbf{K}_\psi^e$, respectively.

Results in Figure 4 clearly show that the exact integration of $\mathbf{K}_t^e$ leads to shear locking as expected. Good (locking-free) results are obtained by one-point reduced integration of the three groups of matrices, as explained in the previous paragraph.

The influence of reduced integration in the distribution of the transverse shear stresses was studied next for the three groups of matrices. Figures 5–7 show the thickness distribution of these stresses in sections located at distances $\frac{L}{20}, \frac{L}{4}, \frac{L}{2}$ and $\frac{3}{4}L$ from the clamped end for slenderness ratios of $\lambda = 5, 10$ and $100$. Results are compared with the plane stress solution and also with results obtained with the standard 2-noded element based on laminated Timoshenko beam theory (labelled TBT in the figures).

The conclusion is that for small values of $\lambda$ the reduced or exact reduced integration of matrix $\mathbf{K}_t^e$ leads to similar results. For slender beams, however, results obtained using reduced integration for $\mathbf{K}_s^e$; $\mathbf{K}_s^e$ and $\mathbf{K}_{s\psi}^e$; and $\mathbf{K}_s^e$, $\mathbf{K}_{s\psi}^e$ and $\mathbf{K}_\psi^e$ are different. Slightly more accurate results are obtained with the second choice for the section at $x = L/4$ and $\lambda = 100$ (Figure 7b).

In conclusion, we recommend using a reduced one-point integration for matrices $\mathbf{K}_s^e$ and $\mathbf{K}_{s\psi}^e$, while matrix $\mathbf{K}_\psi^e$ should be integrated with a 2-point quadrature.

(a) $\tau_{xz}, \lambda = 5, L/20$

(b) $\tau_{xz}, \lambda = 5, L/4$

(c) $\tau_{xz}, \lambda = 5, L/2$
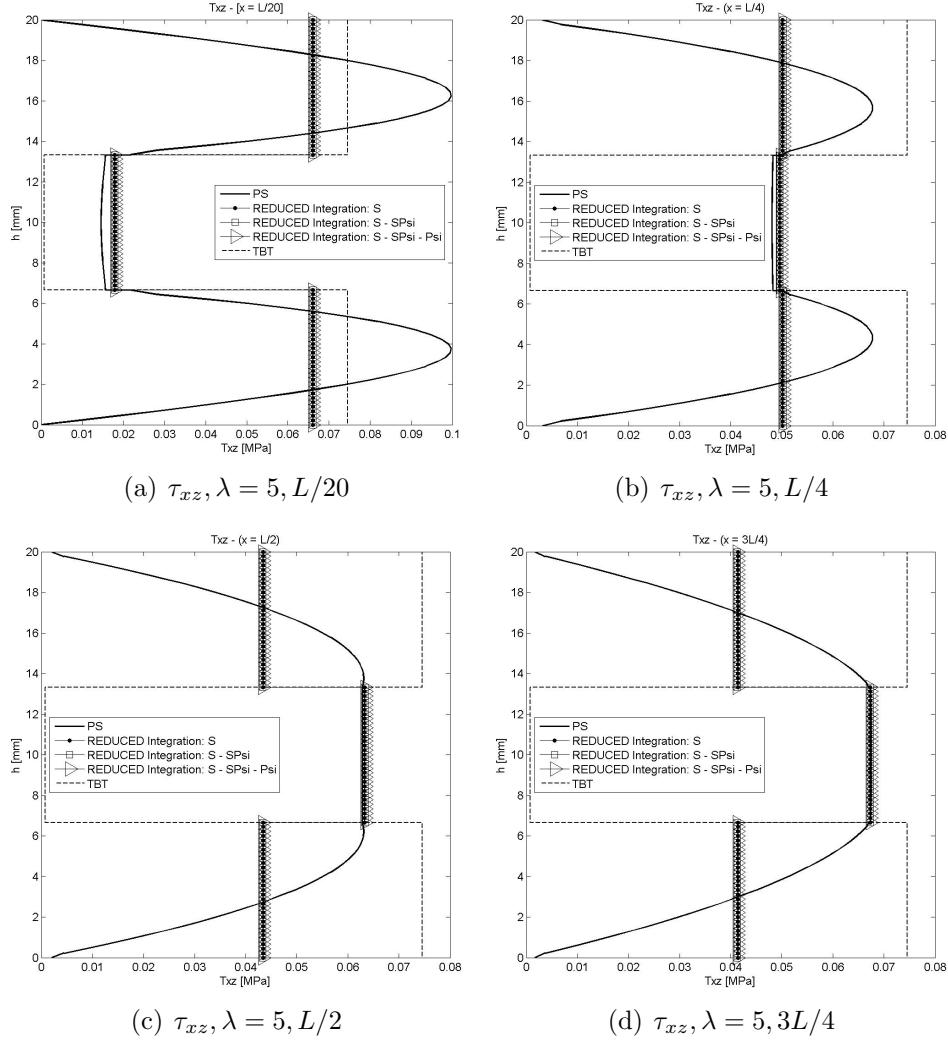
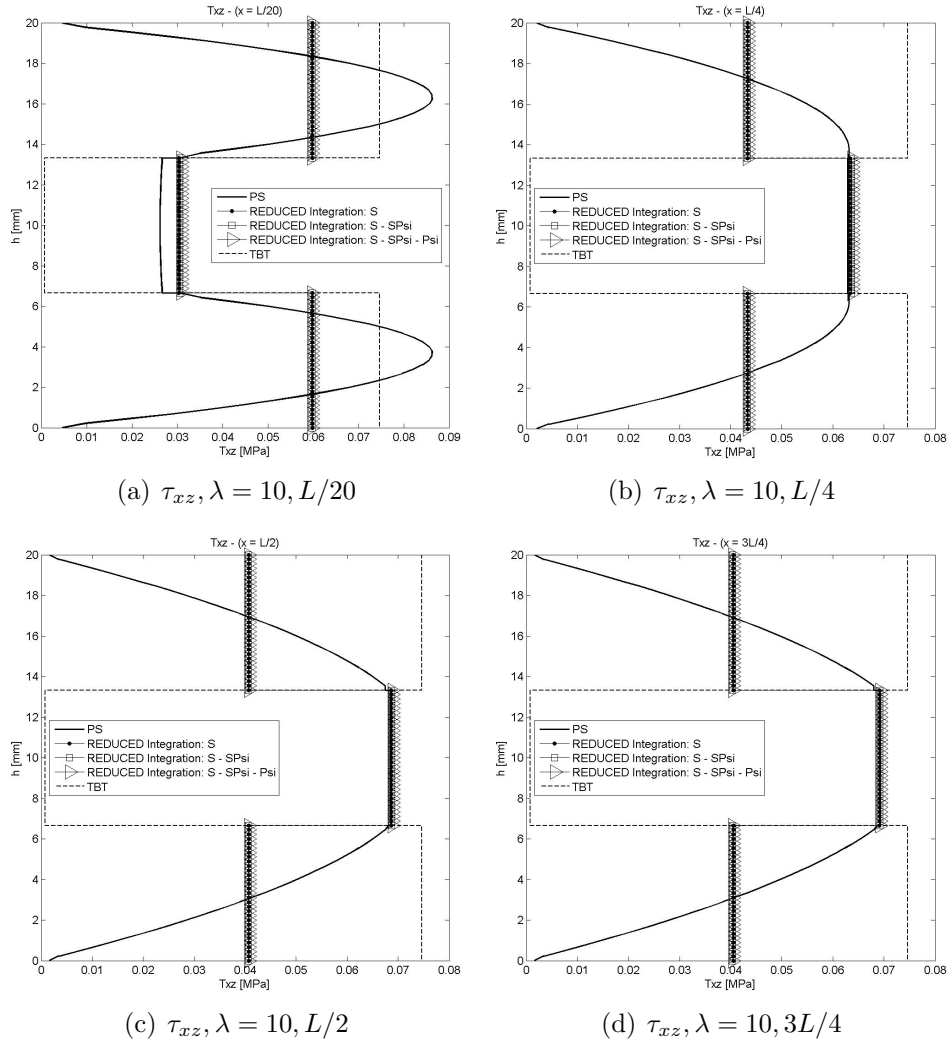(d) $\tau_{xz}, \lambda = 5, 3L/4$

**Figure 5**: Symmetric 3-layered cantilever thick beam under end point load. Thickness distribution of shear stress for $\lambda = 5$ at different sections

## 6   CONVERGENCE STUDY

The same three-layered cantilever beam of Figure 2 was studied next for three different set of thickness and material properties for the three layers as listed in Table 2. Material A is the more homogeneous one, while material C is clearly the more heterogeneous.

The problem was studied with six meshes of LTZZ elements ranging from 5 to 300 elements. Tables 3–5 show the convergence with the number of elements for the deflection and function $\Psi$ at the beam end, the maximum axial stress $\sigma_x$ at the end section and the maximum shear stress $\tau_{xz}$ at the mid section.

Convergence is measured by the relative error defined as

$$e_r = \frac{v_6 - v_i}{v_6} \tag{30}$$

where $v_6$ and $v_i$ are the values of the magnitude of interest obtained using the finest grid (300 elements) and the $i$th mesh ($i = 1, 2, \cdots 5$), respectively.

11

(a) $\tau_{xz}, \lambda = 10, L/20$

(b) $\tau_{xz}, \lambda = 10, L/4$

(c) $\tau_{xz}, \lambda = 10, L/2$

(d) $\tau_{xz}, \lambda = 10, 3L/4$

**Figure 6**: Symmetric 3-layered cantilever thick beam under end point load. Thickness distribution of shear stress for $\lambda = 10$ at different sections

| | | Material properties | | |
|---|---|---|---|---|
| | | **Layer 1**(bottom) | **Layer 2** (core) | **Layer 3** (top) |
| **Composite A** | h [mm] | 6.66 | 6.66 | 6.66 |
| | E [MPa] | 4.4E5 | 2.19E4 | 2.19E5 |
| | G [MPa] | 2.00E5 | 8.80E3 | 8.76E4 |
| **Composite B** | h [mm] | 6.66 | 6.66 | 6.66 |
| | E [MPa] | 2.19E5 | 2.19E3 | 2.19E5 |
| | G [MPa] | 8.76E4 | 8.80E2 | 8.76E4 |
| **Composite C** | h [mm] | 2 | 16 | 2 |
| | E [MPa] | 7.3E5 | 0.0073E5 | 2.19E5 |
| | G [MPa] | 2.92E5 | 0.0029E5 | 0.876E5 |

**Table 2**: Non symmetric 3-layered cantilever beams. Material properties for convergence analysis

Results clearly show that convergence is always slower for the heterogeneous material case, as expected.

For a mesh of 25 elements the errors for all the magnitudes considered are less than 1% for materials A and B. For material C the maximum error does not exceed
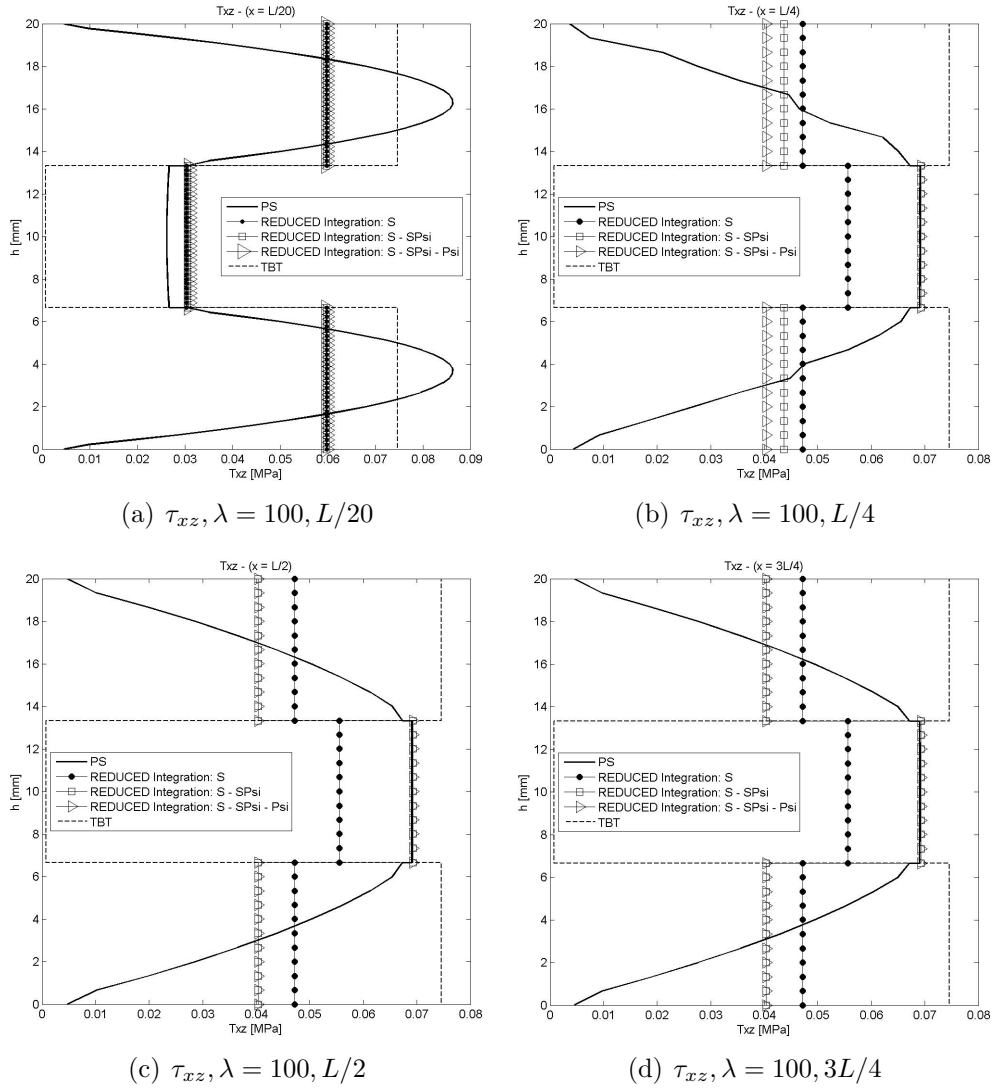
(a) $\tau_{xz}, \lambda = 100, L/20$

(b) $\tau_{xz}, \lambda = 100, L/4$

(c) $\tau_{xz}, \lambda = 100, L/2$

(d) $\tau_{xz}, \lambda = 100, 3L/4$

**Figure 7**: Symmetric 3-layered cantilever thick beam under end point load. Thickness distribution of shear stresses for $\lambda = 100$

| $e_r\% - w$ at $x = L$ | | | |
|---|---|---|---|
| **Number of elements** | **Composites** | | |
| | **A** | **B** | **C** |
| 5 | 1.800 | 9.588 | 42.289 |
| 10 | 0.506 | 2.901 | 19.277 |
| 25 | 0.0860 | 0.499 | 4.913 |
| 50 | 0.0191 | 0.123 | 1.406 |
| 100 | 0.0048 | 0.031 | 0.339 |
| 300 | 0.0000 | 0.0000 | 0.0000 |

**Table 3**: Non symmetric 3-layered cantilever thick beams under end point load ($\lambda = 5$). Relative error for $w$ at $x = L$

5% (Table 6a). For the 50 element mesh errors of the order of 1% or less were obtained in all cases.

Results for a 10 element mesh are good for material A (errors less than 1%),

13

| $e_r\% - \Psi$ at $x = L$ | | | |
|---|---|---|---|
| Number of | Composites | | |
| elements | A | B | C |
| 5 | 0.040 | 8.563 | 36.113 |
| 10 | 0.003 | 1.814 | 8.042 |
| 25 | 0.000 | 0.259 | 0.328 |
| 50 | 0.000 | 0.063 | 0.033 |
| 100 | 0.000 | 0.016 | 0.007 |
| 300 | 0.000 | 0.000 | 0.000 |

**Table 4**: Non symmetric 3-layered cantilever thick beams under end point load ($\lambda = 5$). Convergence study. Relative error for $\Psi$ at $x = L$

(a)                                                                          (b)

| $e_r\% - (\sigma_x)_{\max}$ at $x = L$ | | | |
|---|---|---|---|
| Number of | Composites | | |
| elements | A | B | C |
| 5 | -0.568 | -6.923 | -18.239 |
| 10 | -0.076 | -2.704 | -12.437 |
| 25 | -0.013 | -0.568 | -4.266 |
| 50 | -0.003 | -0.131 | -1.095 |
| 100 | 0.001 | -0.029 | -0.250 |
| 300 | 0.000 | 0.000 | 0.000 |

| $e_r\% - (\tau_{xz})_{\max}$ at $\frac{L}{2}$ | | | |
|---|---|---|---|
| Number of | Composites | | |
| elements | A | B | C |
| 5 | 7.020 | 19.283 | 50.938 |
| 10 | 0.352 | 5.176 | 20.602 |
| 25 | 0.052 | 0.888 | 3.408 |
| 50 | 0.010 | 0.210 | 0.707 |
| 100 | 0.003 | 0.049 | 0.147 |
| 300 | 0.000 | 0.000 | 0.000 |

**Table 5**: Non symmetric 3-layered cantilever thick beams under end point load ($\lambda = 5$). Convergence study. (a) Relative error for the maximum value of $\sigma_x$ at $x = L$ and (b) idem for $\tau_{xz}$ at $x = L/2$

relatively good for material B (errors less than 3%) and unacceptable for material C (errors ranging from 12 to 20%).

## 7 EXAMPLES

### 7.1 Three-layered thick cantilever beam with non symmetric material properties

We present results for a laminated thick cantilever beam under an end point load. The material properties are those of Composite C in Table 2. The slenderness ratio is $\lambda = 5$.

For the laminated sandwich considered the core is eight times thicker than the face sheets. In addition, the core is three orders of magnitude more compliant than the bottom face sheet. Moreover, the top face sheet has the same thickness as the bottom face sheet, but is about three times stiffer. Note that this laminate does not possess material symmetry with respect to the mid-depth reference axis. The high heterogeneity of this stacking sequence is very challenging for the beam theories considered herein to model adequately.

As in previous section, the legend caption PS denotes the *reference* solution obtained with the structured mesh of 27000 four-noded plane stress quadrilaterals shown in Figure 3. TBT denotes the solution obtained with a mesh of 300 2-noded beam elements based on standard laminated Timoshenko beam theory. ZZ-300, ZZ-50, ZZ-25, ZZ-10 refer to the solution obtained with the LTZZ beam element using meshes of 300, 50, 25 and 10 elements, respectively.
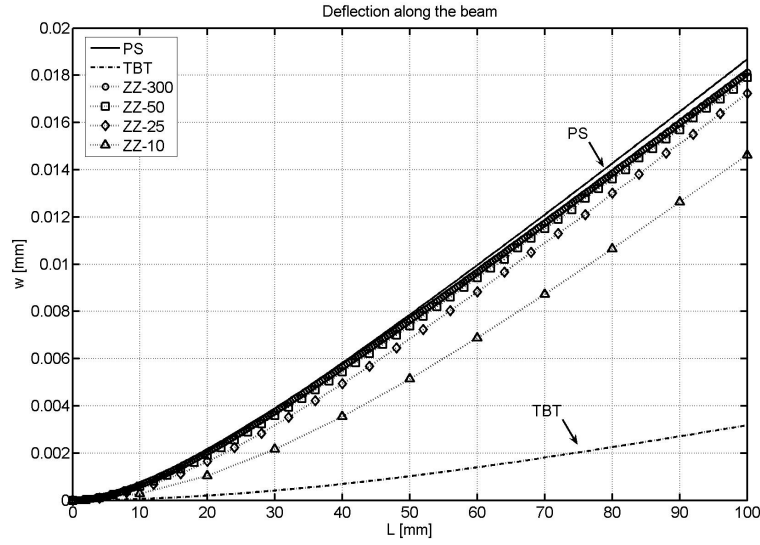
14

**Figure 8**: Non symmetric 3-layered cantilever thick beam under end point load ($\lambda = 5$). Distribution of the vertical deflection $w$ for different theories and meshes
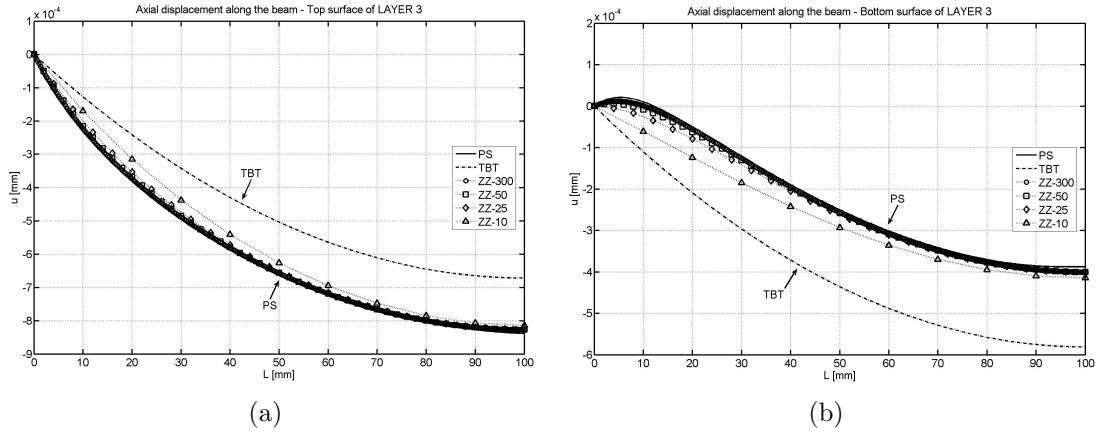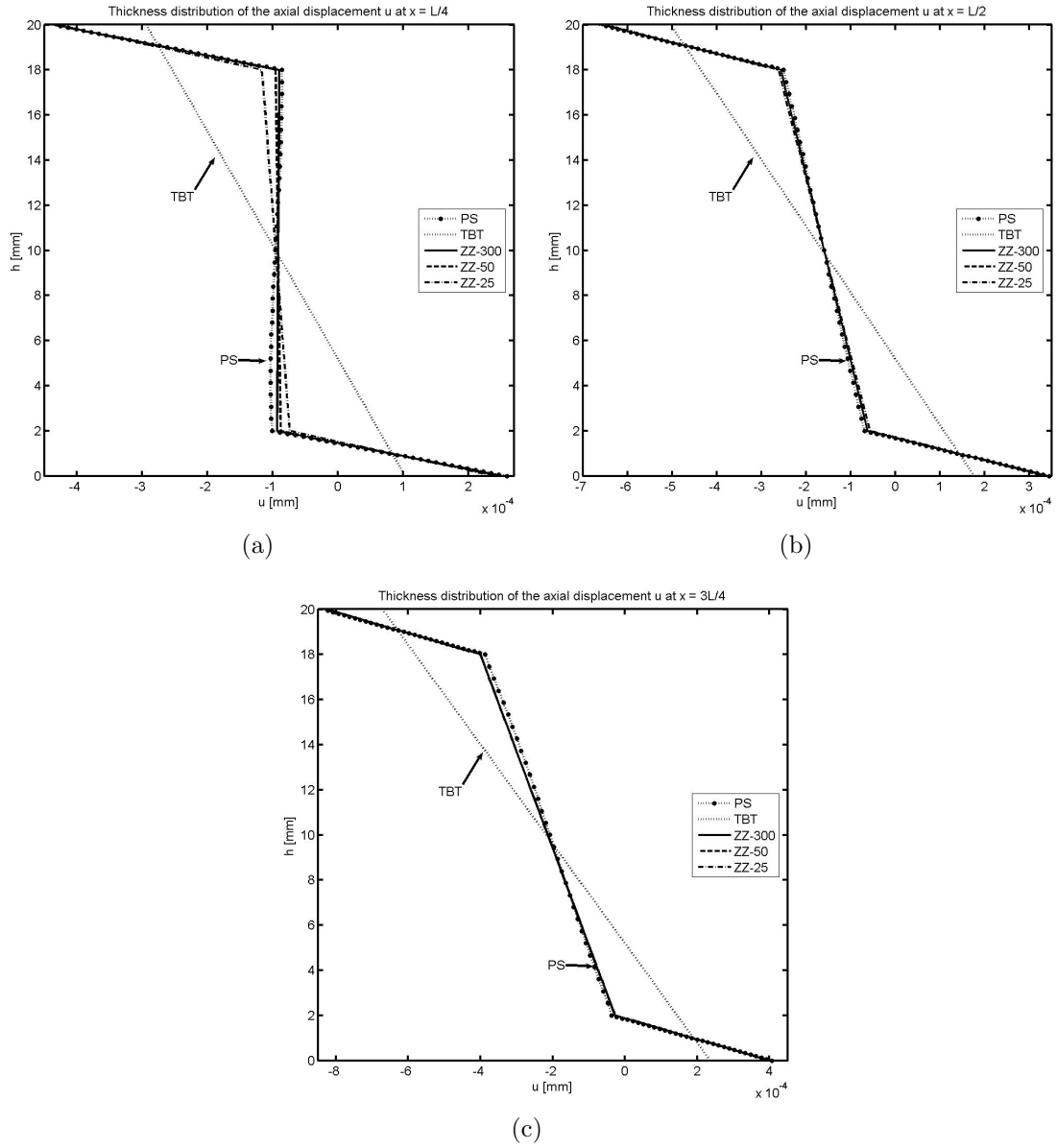


(a)



(b)

**Figure 9**: Non symmetric 3-layered cantilever thick beam under end point load ($\lambda = 5$). Axial displacement $u$ at the upper and lower surfaces of the top layer (layer 3)

Figure 8 shows the deflection values along the beam length. Very good agreement with the plane stress solution is obtained already for the ZZ-50 mesh as expected from the conclusions of the previous section.

It is remarkable that TBT results are considerable stiffer. The difference with the reference solution is about *six times stiffer* for the end deflection value.

Figure 9 shows the distribution of the axial displacements at the upper and lower surfaces of layer 3 (top layer) along the beam length. Excellent results are again obtained with the 50 element mesh, while the TBT results are far from the correct ones.

Figure 10 shows the thickness distribution for the axial displacement at sections located at distances $\frac{L}{4}$, $\frac{L}{2}$ and $\frac{3L}{4}$ from the clamped end. Results for the LTZZ element (ZZ-25, ZZ-50 and ZZ-300) are in good agreement with the reference solution. The
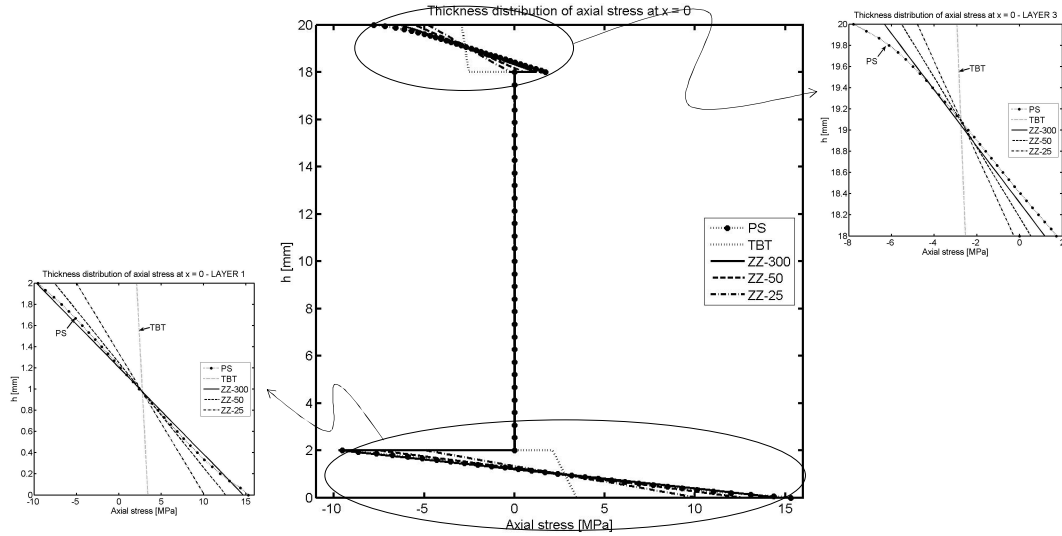
15

**Figure 10**: Non symmetric 3-layered cantilever thick beam under end point load ($\lambda = 5$). Thickness distribution of the axial displacement $u$ at $x = L/4$ (a), $x = L/2$ (b) and $x = L$ (c)

TBT results have the standard linear distribution which is far from the correct zigzag results.

Figure 11 shows the distribution along the beam length of the axial stress $\sigma_x$ at the top and bottom surfaces of the beam cross section. Very good agreement between the reference PS solution and the ZZ-50 and ZZ-300 results is obtained. Results for the ZZ-25 mesh compare reasonably well with the PS solution except in the vicinity of the clamped edge. This error is corrected for the ZZ-50 and ZZ-300 meshes. The TBT results yield a linear distribution of the axial stress along the beam, as expected. This introduces large errors in the axial stress values in the vicinity of the clamped edge, as clearly shown in Figure 11.

16
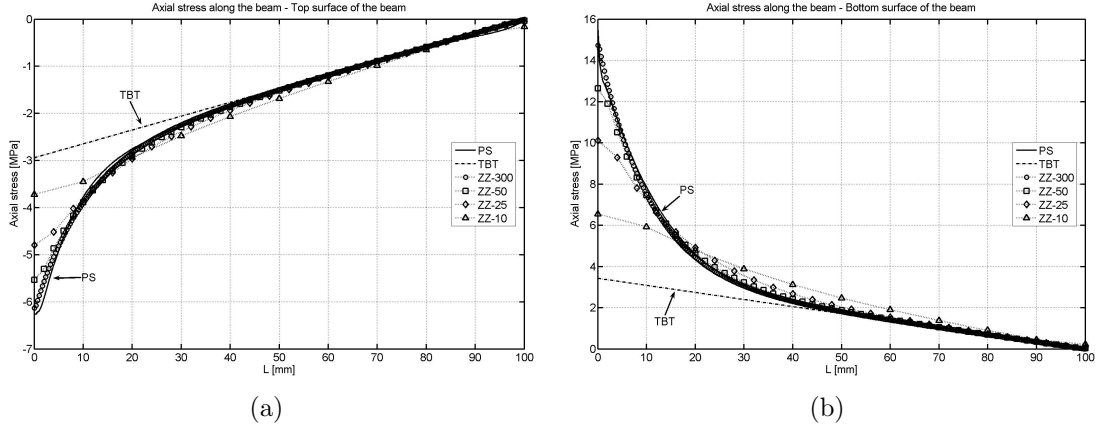
**Figure 11**: Non symmetric 3-layered cantilever thick beam under end point load ($\lambda = 5$). Axial stress $\sigma_x$ at upper (a) and lower (b) surfaces of the cross section along the beam length



**Figure 12**: Non symmetric 3-layered cantilever thick beam under end point load ($\lambda = 5$). Thickness distribution of the axial stress $\sigma_x$ at $x = 0$

Figures 12 and 13 show the thickness distribution for the axial stress $\sigma_x$ at the clamped section and at the center of the beam. The LZZZ results agree quite well with those of the reference solution. The TBT results have an erroneous stress distribution for the top and bottom layers at the clamped end. These differences are less important for the central section.

The distribution of the (constant) tangential shear stress $\tau_{xz}$ for each of the three layers along the beam length is shown in Figure 14. TBT results are clearly inaccurate (except for the values at the clamped edge). Good agreement with the reference solution is obtained for the ZZ-50 and ZZ-300 meshes. Results for the ZZ-10 mesh are quite inaccurate, but still much better than the TBT solution.

Figure 15 shows the thickness distribution for the transverse shear stress $\tau_{xz}$ at different sections ($\frac{L}{20}, \frac{L}{4}, \frac{L}{2}$ and $\frac{3L}{4}$). The LTZZ results provide an accurate estimate of the average transverse shear stress value for each layer.
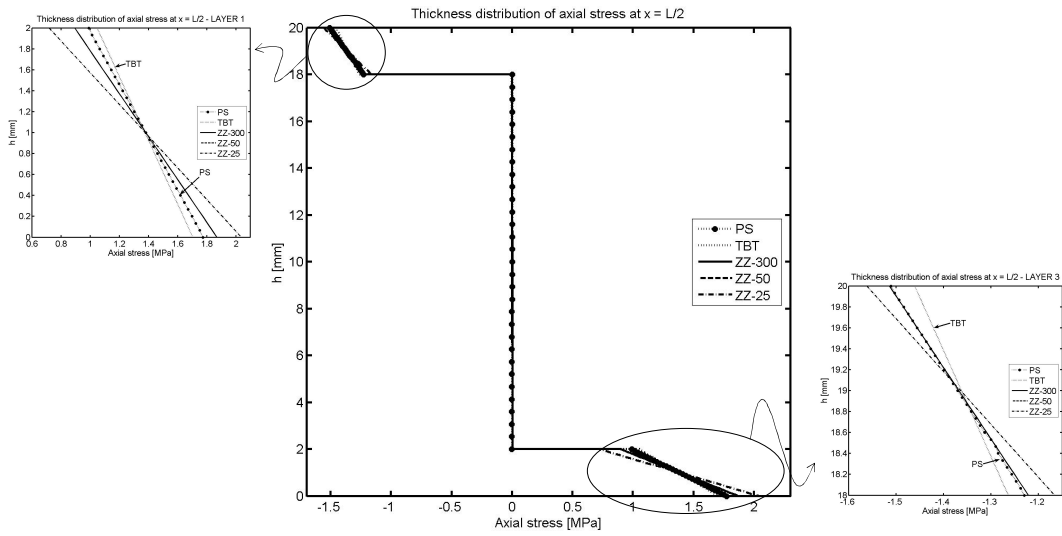
17

**Figure 13**: Non symmetric 3-layered cantilever thick beam under end point load ($\lambda = 5$). Thickness distribution of the axial stress $\sigma_x$ at $x = L/2$
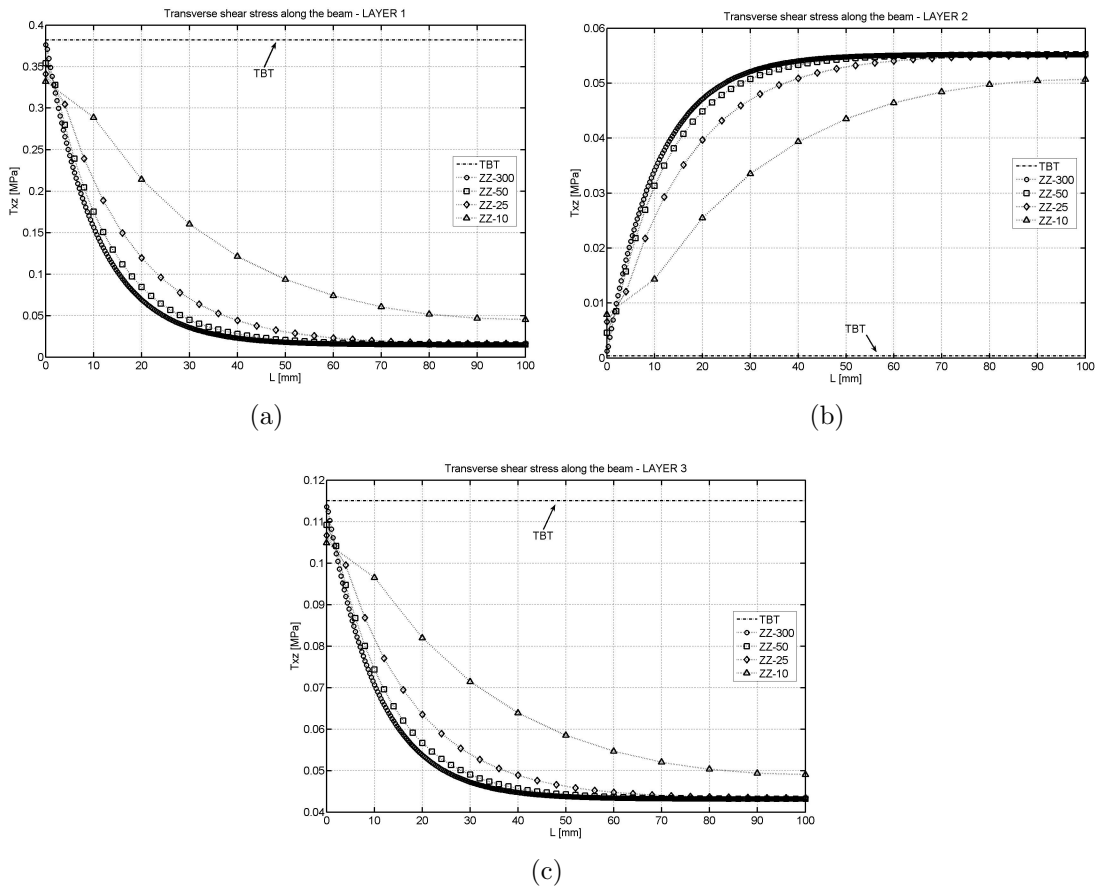


(a)

(b)



(c)

**Figure 14**: Non symmetric 3-layered cantilever thick beam under end point load ($\lambda = 5$). Transverse shear stress $\tau_{xz}$ along the beam. Layer 1 (a), layer 2 (b) and layer 3(c)
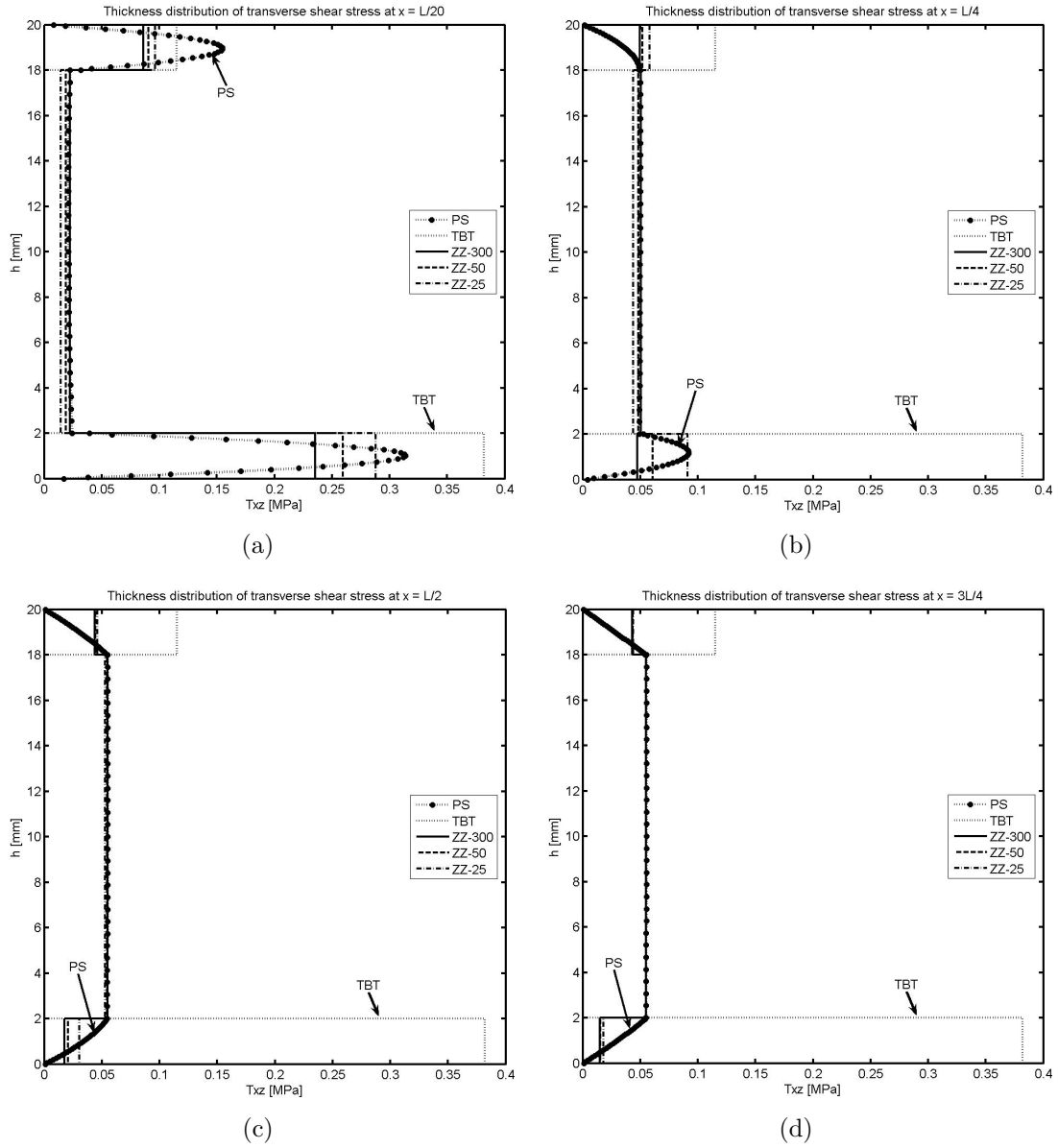
Figure 15: Non symmetric 3-layered cantilever thick beam under end point load ($\lambda = 5$). Thickness distribution of transverse shear stress $\tau_{xz}$ at $L/20$ (a), $L/4$ (b), $L/2$ (c) and $3L/4$ (d)

The TBT results are acceptable for the central layer and clearly overestimate the transverse shear stress in sections far from the clamped end.

## 7.2 Three-layered simple supported (SS) thick beams under uniform load

The next example is the analysis of a three-layered simple supported thick beam under a uniformly distributed load. The material properties and the thickness for the three layers are shown in Table 6. The material has a non symmetric distribution with respect to the beam axis. The material of the core has properties close to those of the third (top) layer in this case. The slenderness ratio is $\lambda = 5$. Results

19

| | Thickness and material properties | | |
|---|---|---|---|
| | Layer 1 (bottom) | Layer 2 (core) | Layer 3 (top) |
| h [mm] | 6.6666 | 6.6666 | 6.6666 |
| E [MPa] | $2.19\text{E}^5$ | $5.30\text{E}^5$ | $7.30\text{E}^5$ |
| G [MPa] | $8.76\text{E}^5$ | $2.90\text{E}^2$ | $2.92\text{E}^5$ |

**Table 6**: Thickness and material properties for 3-layered non-symmetric simple supported (SS) beam
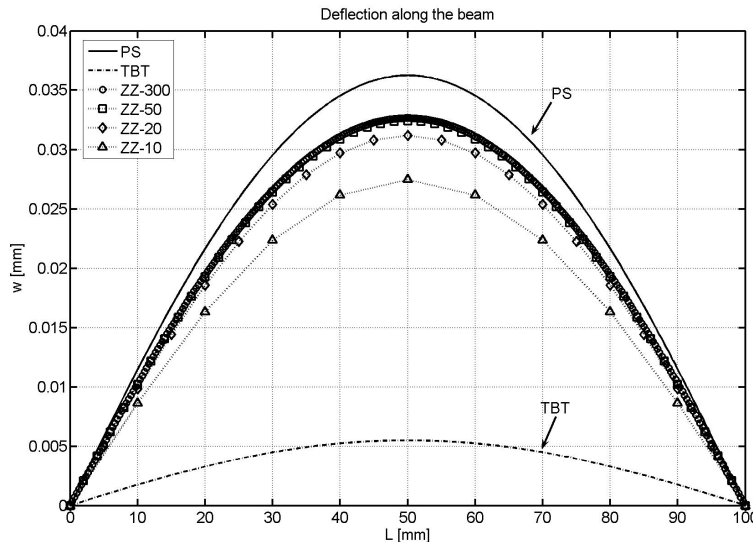


**Figure 16**: Non symmetric 3-layered SS thick beam under uniformly distributed load ($\lambda = 5$). Distribution of vertical deflection $w$ along the beam length

obtained with the LTZZ element are once more compared with those obtained with a mesh of 300 2-noded TBT elements and with the mesh of 27000 4-noded plane stress (PS) rectangles shown in Figure 3. The PS solution has been obtained by fixing the vertical displacement of all nodes at the end sections and the horizontal displacement of the mid-line node at $x = 0$ and $x = L$ to a zero value.

No advantage of the symmetry of the problem for the discretization has been taken.

Figure 16 shows the distribution of the vertical deflection for the different methods. The error in the "best" maximum central deflection value versus the "exact" PS solution is $\simeq 12\%$. The discrepancy is due to the difference in the way the simple support condition is modelled in beam and PS theories, as well as to the limitations of beam theory to model accurately very thick beams. The TBT results are very inaccurate, as expected.

Figure 17 shows the distribution of the axial stress $\sigma_x$ along the beam for the top surface of the second and third layer.

The accuracy of the LTZZ results is remarkable with a maximum error of 10% despite of the modeling limitations mentioned above. The TBT results are incorrect.

The accuracy of the LTZZ results is even better for the distribution of the shear stress $\tau_{xz}$ along the beam in each of the three layers (Figure 18). The TBT results
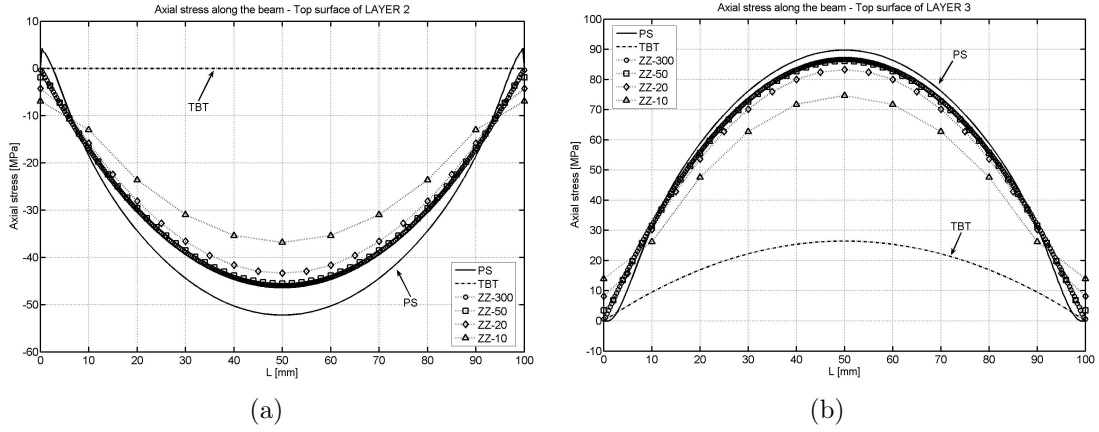
**Figure 17**: Non symmetric 3-layered SS thick beam under uniformly distributed load ($\lambda = 5$). Distribution of axial stress $\sigma_x$ at upper surface of layer 2 (a) and layer 3 (b)
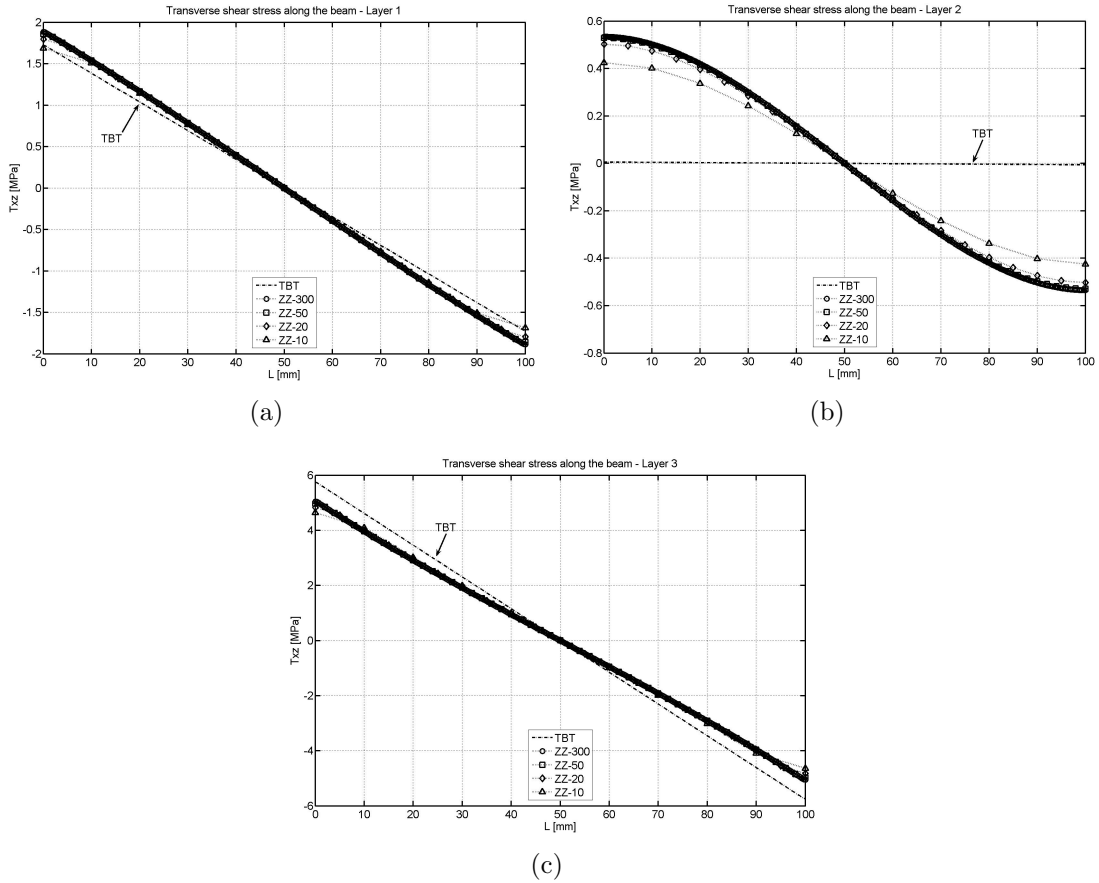


**Figure 18**: Non symmetric 3-layered SS thick beam under uniformly distributed load ($\lambda = 5$). Distribution of shear stress $\tau_{xz}$ along the beam for layer 1 (a), layer 2 (b) and layer 3 (c)

are accurate for the first and third layer but are wrong for the core layer.

Figure 19 shows the thickness distribution of the axial displacement at the left end and mid sections. The LTZZ element captures very well the zigzag shape of the axial displacement field even for a coarse mesh of 10 elements. The TBT element
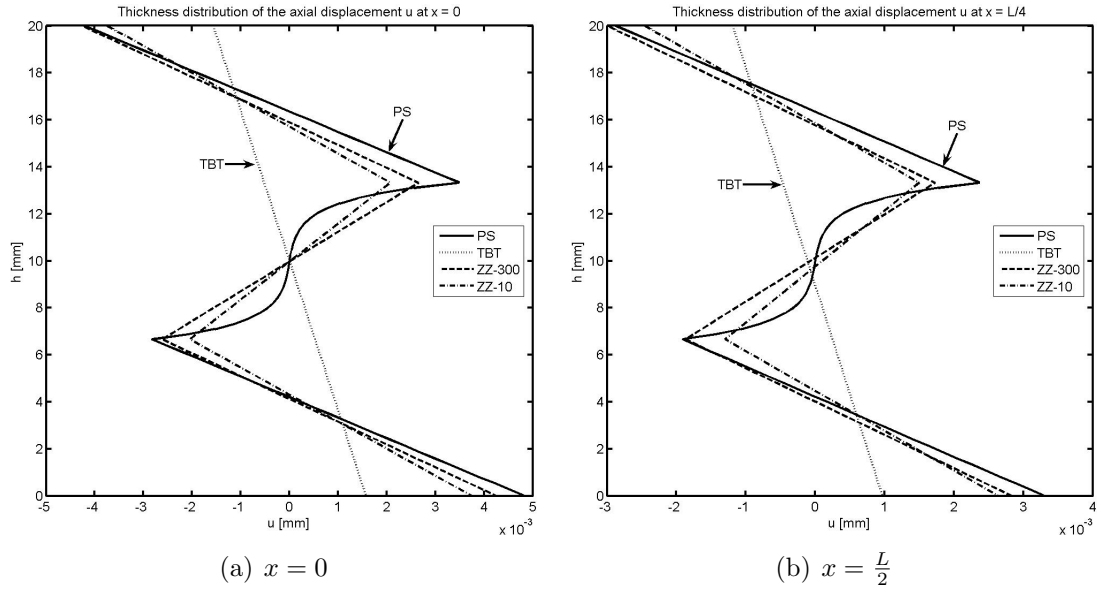
21

(a) $x = 0$             (b) $x = \frac{L}{2}$

**Figure 19**: Non symmetric 3-layered SS thick beam under uniformly distributed load ($\lambda = 5$). Thickness distribution of axial displacement at $x = 0$ (a) and at $x = L/2$ (b)
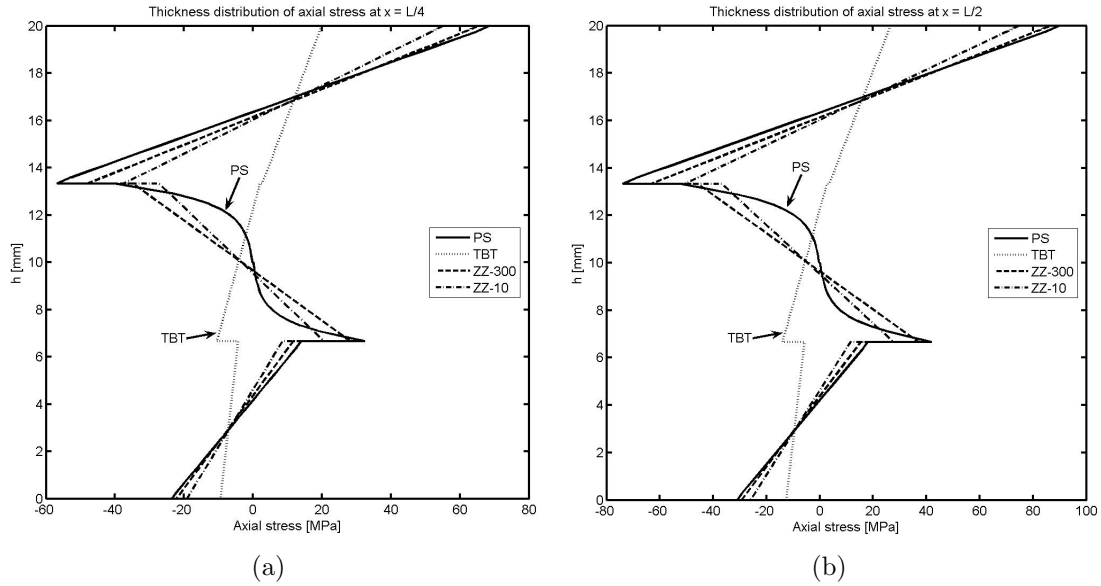


(a)               (b)

**Figure 20**: Non symmetric 3-layered SS thick beam under uniformly distributed load ($\lambda = 5$). Thickness distribution of axial stress $\sigma_x$ at $x = 0$ (a) and at $x = L/2$ (b)

yields an unrealistic linear distribution.

Figures 20 and 21 show the thickness distribution of the axial stress and the transverse shear stress at the left end and mid sections. The accuracy of the LTZZ results is again noticeable (even for the coarse 10 element mesh). The TBT element fails to capture the zigzag distribution of the axial stress (Figure 20) and gives a wrong value of almost zero shear stress at the core layer for the two sections chosen (Figure 21).
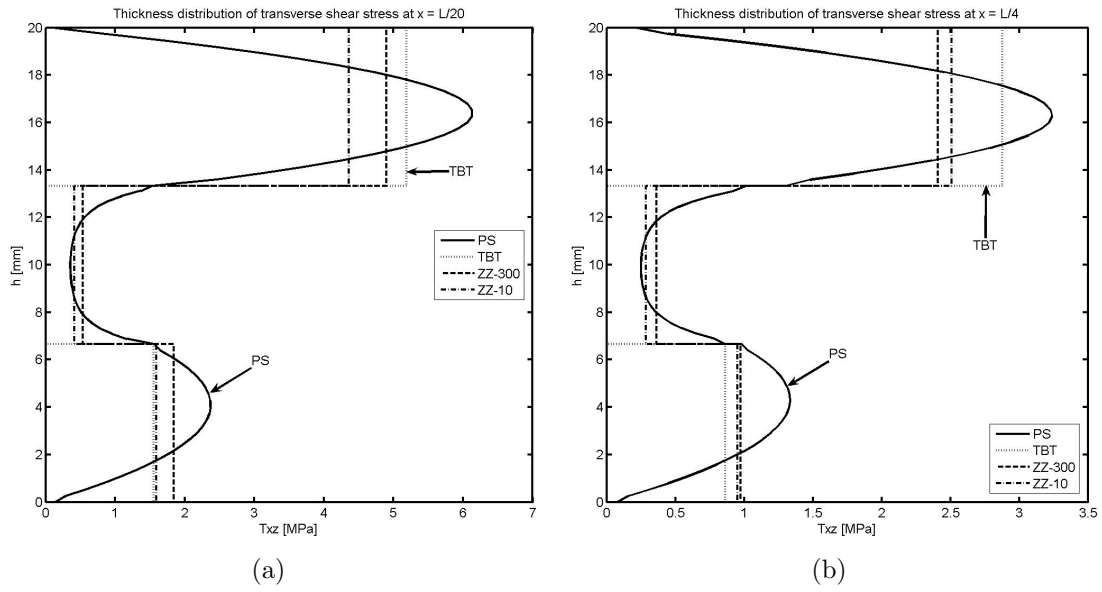
**Figure 21**: Non symmetric 3-layered SS thick beam under uniformly distributed load ($\lambda = 5$). Thickness distribution of the shear stress at $x = L/20$ (a) and at $x = L/4$ (b)
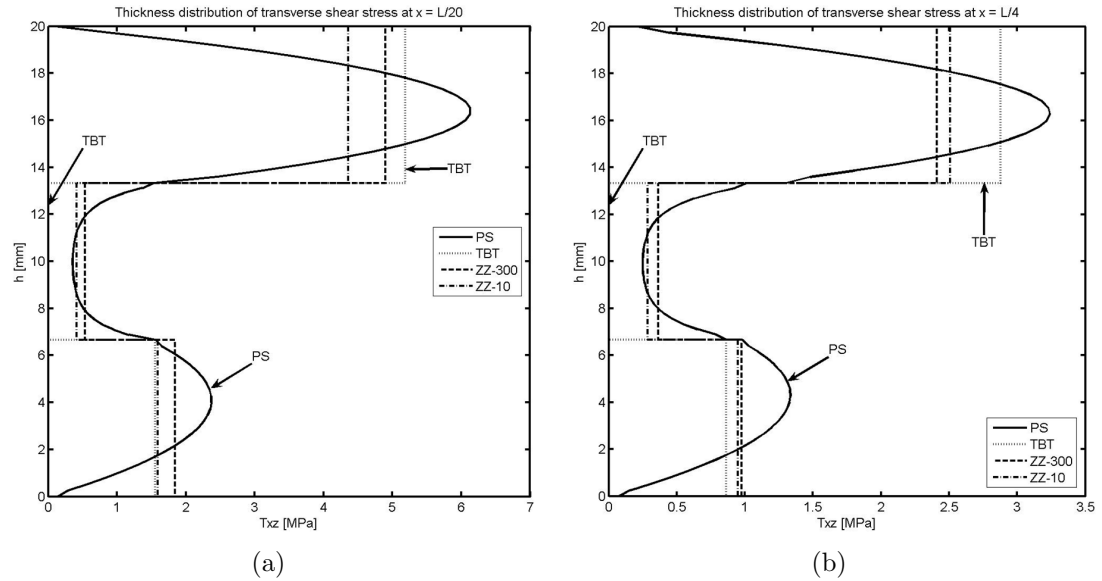


**Figure 22**: Non symmetric 3-layered SS moderately thick beam under uniformly distributed load ($\lambda = 10$). Distribution along the beam length of the vertical deflection $w$ (a) and the axial stress $\sigma_x$ at the upper of layer 2 (b)

Figure 22 shows a similar set of results for a moderately thick beam with $\lambda = 10$ and the same material properties. Results shown are the distribution along the beam of the deflection and the axial stress at the top surface of layer 2. The accuracy of the TBT element and its superiority versus the TBT one shows even clearer in this case.

23

## 8   CONCLUSIONS

We have presented a simple and accurate 2-noded beam element based on the combination of Timoshenko beam theory with the refined zigzag kinematics proposed by Tessler et al. [19]. The element has four degrees of freedom per node (the axial displacement, the deflection, the rotation and the amplitude of the zigzag function). A standard $C^\circ$ interpolation is used for all variables, as it is typical in Timoshenko beam elements. The resulting LTZZ element is shear locking-free and has shown an excellent behaviour for analysis of thick and thin composite beams with clamped and simple supported conditions. Numerical results match in most cases those obtained with a two-dimensional plane-stress FEM using a far larger number of degrees of freedom. It is remarkable that the zigzag distribution of the axial displacement across the thickness typical of composite beams is very accurately captured with the simple approximation chosen. The superiority of the LTZZ element versus the standard 2-noded Timoshenko beam element has been clearly shown for all the examples presented in the paper.

## 9   ACKNOWLEDGEMENTS

## REFERENCES

[1] Timoshenko S. On the correction for shear of differential equations for transverse vibrations of prismatic bars. Philosophical Magazine Series, Vol. 41, pp. 744-746, 1921.

[2] Liu D. and Li X. An overall view of laminate theories based on displacement hypothesis. Journal of Composite Materials, Vol. 30(14), pp. 1539-1561, 1996.

[3] Sun C.T. and Whitney J.M. Theories for the dynamic response of laminated plates. AIAA Journal, Vol. 11(2), pp. 178-183, 1973.

[4] Di Sciuva M. An improved shear-deformation theory for moderately thick multilayered anisotropic shells and plates. ASME Journal of Applied Mechanics, Vol. 54, pp. 589-596, 1987.

[5] Owen D.R.J. and Li Z.H., A refined analysis of laminated plates by finite element displacement methods. Part I. Fundamentals and static analysis. II Vibration and stability. Comp. Struct, Vol. 26, pp. 907–923, 1987.

[6] Botello, S. Oñate, E. and Canet, J.M., A layer-wise triangle for analysis of laminated composite plates and shells. Computers and Structures, Vol. 70, 635–646, 1999.

[7] Di Sciuva M. A refined transverse shear deformation theory for multilayered anisotropic plates. Atti Accademia delle Scienze di Torino, Vol. 118, pp. 279-295, 1984.

[8] Di Sciuva M. Bending, vibration and buckling of simply supported thick multi-layered orthotropic plates: an evaluation of a new displacement model. Journal of Sound and Vibration, Vol. 105, pp. 425-442, 1986.

[9] Murakami H. Laminated composite plate theory with improved in-plane responses. ASME Journal of Applied Mechanics, Vol. 53, pp. 661-666, 1986.

[10] Di Sciuva M. Development of an anisotropic, multilayered, shear-deformable rectangular plate element. Computers and Structures, Vol. 21(4), pp. 789-796, 1985.

[11] Di Sciuva M. Further refinement in the transverse shear deformation theory for multilayered composite plates. Atti Accademia delle Scienze di Torino, Vol. 124(5-6), pp. 248-268, 1990.

[12] Di Sciuva M. Multilayered anisotropic plate models with continuous interlaminar stresses. Composite Structures, Vol. 22(3), pp. 149-168, 1992.

[13] Averill R.C. Static and dynamic response of moderately thick laminated beams with damage. Composites Engineering, Vol. 4(4), pp. 381-395, 1994.

[14] Averill R.C. and Yuen Cheong Yip. Development of simple, robust finite elements based on refined theories for thick laminated beams. Computers & Structures, Vol. 59(3), pp. 529-546, 2006.

[15] Alam N.M. and Upadhyay N.Kr. Finite element analysis of laminated composite beams of zigzag theory using MATLAB. Int. J. of Mechanics and Solids, Vol. 5(1), pp. 1–14, 2010.

[16] Savoia M. On the accuracy of one-dimensional models for multilayered composite beams. Int. J. Solids Struct., Vol. 33, pp. 521-44, 1996.

[17] Kapuria S, Dumir P.C. and Jain N.K. Assessment of zigzag theory for static loading, buckling, free and forced response of composite and sandwich beams. Composite Structures, Vol. 64, pp. 317-27, 2004.

[18] Kapuria, S., Dumir, P.C., Ahmed, A. and Alam, N. Finite element model of efficient zigzag theory for static analysis of hybrid piezoelectric beams, Computational Mechanics, Vol. 34 (6), pp. 475–483, 2004.

[19] Tessler, A., Di Sciuva M. and Gherlone, M. A refined zigzag beam theory for composite and sandwich beams. J. of Composite Materials, Vol. 43, 1051–1081, 2009.